Three-dimensional photonic crystals with an active surface: Gold film terminated opals

Boyang Ding,[1] Martyn E. Pemble,[1] Alexander V. Korovin,[2] Ulf Peschel,[2] and Sergei G. Romanov[2,3,*]
[1]*Tyndall National Institute, Prospect Row, Cork, Ireland*
[2]*Institute of Optics, Information and Photonics, University of Erlangen-Nuremberg, Günther-Scharowsky-Str. 1, 91058 Erlangen, Germany*
[3]*Ioffe Physical Technical Institute, Polytekhnicheskaya Street 26, 194021 St. Petersburg, Russia*
(Received 4 May 2010; published 22 July 2010)

A hybrid metal-dielectric photonic crystal, a thin opal slab coated by a gold film, has been designed in order to exercise additional control upon the light propagation in a photonic band-gap material using extraordinary optical transmission in the corrugated gold film. The photonic and plasmonic components of the hybrid crystal are closely linked, because the photonic crystal lattice provides a spatial template for the gold film corrugation and modifies the electromagnetic vacuum in the vicinity of the gold film. Due to coupling of light diffracted in the opal lattice to surface plasmon polaritons in the metal film, the spectra and angle diagrams of transmission in hybrid structures deviate from the linear superposition of transmission functions of both hybrid components. In particular, the selective conversion of diffraction minima, and cavity mode and thickness dependence of the surface plasmon polariton-related properties have been observed. The synergy of three resonance mechanisms behind the functionality of hybrid photonic crystals provides a uniquely broad tunability of their optical properties.

DOI: 10.1103/PhysRevB.82.035119 PACS number(s): 42.70.Qs, 78.67.Pt

I. INTRODUCTION

Since the invention of photonic crystals (PhCs) special attention has been paid to the control exerted on their properties by changing the lattice symmetry, refractive index contrast, filling fraction of heavy dielectric, and so on. However, despite the fact that the surface of a PhC is the part that directly mediates light coupling to the PhC interior, until recently, the surfaces of three-dimensional (3D) PhCs have not been a focus of interest[1–3] because in general such surfaces cannot support surface modes unless specially terminated[4–6] and truly evanescent waves do not contribute to the PhC optical response.

With the introduction of photonic heterocrystals[7,8] the surface states formed at the heterojunction have been shown to influence interface light coupling.[9] However, the existence of evanescent waves at the interface is limited to the spectral range of photonic band-gap (PBG) overlap[10,11] for the components of the heterostructure. If, instead, the interface is designed to support evanescent waves on its own, the influence of a surface upon PhC properties can be dramatically enhanced. Surface plasmon polariton (SPP) bounded to the metal-dielectric interface is the most likely example of such excitations.

Coating the ordered arrays of submicrometer-size dielectric spheres[12,13] with thin metal films is often used as arguably the simplest and cheapest method of creating regularly corrugated metal films. The close analogy to such hybrid architectures is the metal film with an array of subwavelength holes that exhibit the remarkable phenomenon of extraordinary transmission (EOT).[14,15] Alternative analogy is periodically corrugated metal films possessing similarly anomalous transmission spectrum.[16,17] The reason for EOT is the grating-assisted excitation of coupled SPP on opposite interfaces of a metal film and subsequent radiative decay of the propagating plasmons.

Integrating colloidal crystals with corrugated metal films has been driven so far by the idea to achieve and modify the EOT phenomenon. Therefore, the most frequently studied system was a monolayer of regularly packed nanospheres or a two-dimensional (2D) PhC slab, coated with thin metal film.[18–20] In such architecture the EOT phenomenon becomes relatively stronger[21] because the electromagnetic (EM) field is confined to PhC eigenmodes in contrast to the plane-wave illumination of standing alone perforated metal films. In such a hybrid metal film-2D PhC structure, the overall transmission decreases but the minimum in the transmission spectrum of 2D PhC slab is effectively replaced with the transmission passband after coating with metal, i.e., the metal coating completely alters the properties of a hybrid 2D PhC.

In this work we pursue the different aim, namely, we propose here that deposition of a metal film on a 3D PhC template could provide yet another means of tailoring the PhC properties [Fig. 1(a)]. In fact, this approach allows integrating functionalities of the 3D photonic and 2D plasmonic band-gap crystals in one material. In the case of such hybrid structures one can expect a combination of different optical phenomena. First, the PBG structure should be essentially preserved, because the metal film cannot alter the diffraction of light throughout the depth of 3D PhC. Second, the SPP can be excited in a metal coating due to diffractive coupling and, thus, the EOT bands should appear on top of the standard transmission spectrum of the opal film. Third, the complex topology of the metal coating that is composed of interconnected metal caps can lead to additional resonances. The crucial question to be asked is whether the behavior of the hybrid structure will obey a linear superposition of properties of plasmonic and photonic crystal components or whether the novel functionality can arise from interaction of these components?

In order to address this issue we have prepared the hybrid metal-PhC consisted of a gold film deposited on a surface of a thin opal film. The optical transmission of the bare and

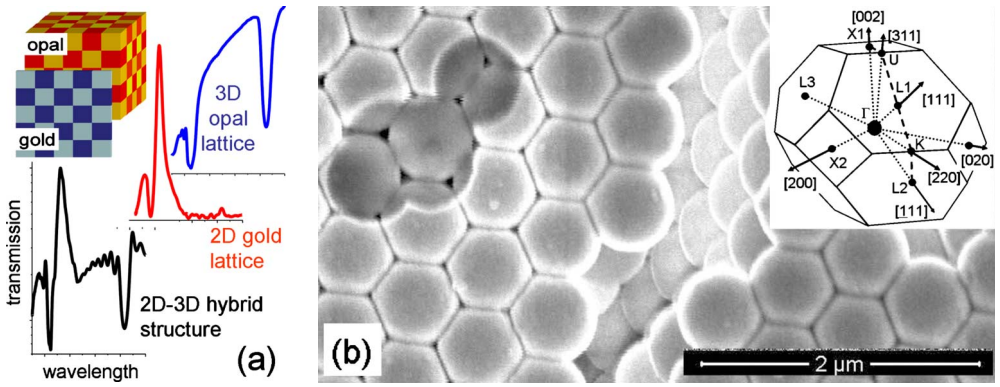

FIG. 1. (Color online) (a) Schematics of the transmission spectrum transformation associated with the formation of the hybrid Au-opal photonic crystal. (b) Scanning electron microscope (SEM) image of opal crystal assembled from 560 nm PMMA spheres coated with 50-nm-thick Au layer. The crack reveals the 3D arrangement of spheres. The shadow on the left side was formed by extra spheres residing during the course of Au coating on the opal surface. The openings between touching spheres in the shaded region are larger than in coated regions thus showing the contribution of a metal film. Inset: the Brillouin zone of the fcc lattice and related wave vectors for different opal crystal planes.

Au-coated opal crystals has been measured over a broad range of the light incidence angles in order to investigate the dispersion of optical resonances. A cumulative effect of the overall transmission reduction due to high reflectivity of a metal film, the transmission attenuation in diffraction resonances, and the transmission enhancement in passbands defined by SPP coupling has been achieved. Moreover, we observed the conversion of transmission minima associated with several diffraction resonances into transmission passbands and the transmission enhancement in the range of (111) diffraction resonance. Overall, our experiments demonstrate possibilities for tuning the spectra and angle diagrams of transmission in hybrid 3D PhCs respective to bare 3D PhC templates by applying the thin metal film on the PhC surface and, further, by changing the properties of the metal film.

II. EXPERIMENTAL TECHNIQUE

Opal films were crystallized in a vertically moving meniscus on hydrophilic glass slides, which were lifted up and out of a suspension of polymethyl methacrylate spheres of diameter 560 nm as described elsewhere[22] using acoustic noise agitation of the colloid suspension during the course of film crystallization in order to improve the ordering of the colloidal crystal structure.[23] Optical characterization of bare opal films yields results that are similar to those reported previously.[23] Nominally 20-, 50-, and 100-nm-thick Au films were sputtered on the freshly crystallized opal [Fig. 1(b)]. The typical sample size was about $2-4$ cm^2. The metal film acquires a form of metal caps on top of opal spheres. These metal caps are electrically connected throughout a film, thus allowing for direct conductivity. Therefore, such metal films acquire a complex topology, being 2D corrugated with the periodicity of the (111) plane of the opal lattice and simultaneously possessing a lattice of through holes of subwavelength size. The hole size and the corrugation depth depend on the thickness of metal coating.

Angle-resolved transmission spectra were acquired at different angles of incidence, θ, with respect to the film normal from $-40°$ to $40°$ with $2°$ step or in a broader angle range from $-80°$ to $80°$ with a $5°$ step. The samples were illuminated by a collimated beam of white light with a diameter of ~ 1 mm obtained from a tungsten lamp. The spectra were acquired using *s*- and *p*-polarized light, the electrical field of which is oriented either perpendicular or parallel to the plane of light incidence, respectively. The control of the azimuthal orientation of this plane allowed the interrogation of the optical properties along the *XULKL* line on the surface of the first Brillouin zone of the opal PhC [inset in Fig. 1(b)] by changing the incidence angle. A depolarizer plate was used to scramble the light polarization before approaching the spectrometer. Ocean Optics charge-coupled device spectrometers were used to record the spectra; the calibration of sample transmission was made with respect to the air.

In what follows we will denote the diffraction resonances in the opal film according to the Miller indices of an fcc lattice for corresponding lattice planes. The most densely packed (111) planes represent the hexagonal lattice of touching spheres. This plane forms the surface of the opal film. The dispersion of diffraction resonances for different families of opal crystal planes was obtained using the Bragg law approximation and the dispersion of the SPP waves was obtained taking into account the dielectric constant of gold.[24]

III. TRANSMISSION SPECTRA OF HYBRID PHOTONIC CRYSTALS

Transmission spectrum of the Au-opal hybrid sample with 50-nm-thick metal coating obtained at the normal incidence of the light is compared in Fig. 2(a) with spectra of its components, namely, the bare opal and the 50nm-thick planar Au film. The spectrum of the opal film shows two minima that correspond to the diffraction resonances at (111) planes and the degenerate resonance associated with the diffraction at (200), (220), and (222) planes of the opal lattice.[23] After coating with an Au film, the long-wavelength transmission of

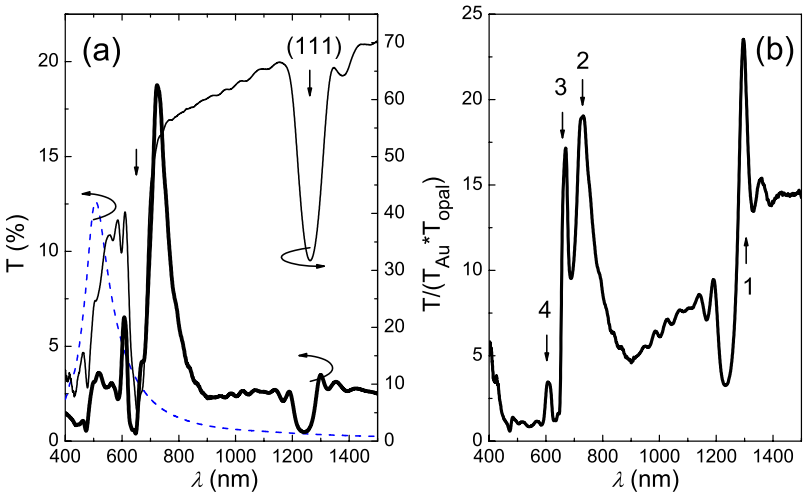

FIG. 2. (Color online) (a) Transmission spectra of the bare opal (thin line), 50-nm-thick plane Au film (dashed line), and Au-opal hybrid structure with 50-nm-thick Au coating (thick line) obtained at $\theta=0°$. Arrows show the transmission minima in the spectrum of bare opal that are associated with diffraction resonances. (b) The transmission spectrum of hybrid structure after its normalization to transmission spectra of the opal template and the planar Au film.

the hybrid structure is reduced by ~30 times due to the high reflectance of the Au film, but it retains the minima of the opal template. Oppositely to the monotonous transmission decrease toward shorter wavelengths in the bare opal film, the transmission of the Au-opal hybrid shows a small peak at the edge of the (111) diffraction resonance minimum and, then, its transmission achieves a value of 19% in the peak at 725 nm. This is followed by another peak at 605 nm [Fig. 2(a)]. The transmission of the Au film of the same nominal thickness increases with the wavelength decrease and achieves a maximum at ~508 nm. This maximum corresponds to the interband transitions in the metal.[25]

It is instructive to normalize the spectrum of Au-opal hybrid to spectra of both of its components [Fig. 2(b)]. This normalized spectrum reveals several bands of the relative transmission enhancement that do exist neither in the opal film nor in the plain metal film. These bands occur in a hybrid structure due to the metal film-to-PhC interaction. The origin of these bands will be discussed later.

Extended comparison of transmission spectra of the bare opal and the Au-opal hybrid structure can be made by plotting the maps of the transmission spectra obtained at different incidence angles under *p*- and *s*-polarized light (Fig. 3). The dark areas correspond to transmission minima and bright areas correspond to the transmission passbands. From the Bragg approximation to the dispersion of the (111) diffraction resonance in the spectra of the bare opal [Fig. 3(b)], the sphere diameter and the effective refractive index were estimated to be $D=560$ nm and $n_{eff}=1.38$. Using these values, the dispersions of $(\bar{1}11)$, (200), (220), (311), and (222) resonances in the fcc lattice were calculated using the Bragg law

$$\lambda_{hkl} = 2d_{hkl}n_{eff}\sqrt{1-\sin^2 r_{hkl}}, \tag{1}$$

where $d_{hkl}=\sqrt{2}D/\sqrt{(h^2+k^2+l^2)}$ is the interplane distance for the (hkl) planes and the internal angle of incidence, r_{hkl}, relates to the external angle via Snell law $n_{eff}\sin(r_{111})=n_{air}\sin(\theta)$.

We then plotted all diffraction resonance dispersions in Figs. 2(a) and 2(b) on top of the transmission map. The mirror asymmetry of the opal PBG structure along the *XULKL* line was disregarded in order to take into account the internal reflections of the probe beam at the opal film boundaries[26] and the lattice twinning due to stacking faults along the [111] axis.[27] Then the good agreement between the dispersions of diffraction resonances in the fcc lattice and experimentally obtained transmission minima was achieved for most of resonances except the band anticrossing directions.

The transmission maps of Au-opal hybrid structure [Figs. 3(c) and 3(d)] differ dramatically from those of the opal template [Figs. 3(a) and 3(b)]. The major features of the hybrid spectra are the transmission minima in correspondence to those of the bare opal and the transmission passbands with their maximum at 725 nm for the normal light incidence. With increasing angle of incidence, the magnitude of the transmission passband decreases rapidly; however, this peak is surrounded by several other transmission bands of lower intensities, the spectral position of which changes with the angle of incidence.

It is readily seen that the dispersion of passbands in Fig. 3(c) correlates directly with the dispersion of SPP resonances. The SPP resonance branches of the 2D hexagonal lattice of holes in the planar Au film are described by the equation

$$k(\omega)\sin\theta = \pm\sqrt{k_{SPP}(\omega)^2-\left(\frac{2\pi}{D\sqrt{3}}(2j-i)\right)^2}-\frac{2\pi i}{D},$$
$$i,j=0,\pm1,\pm2,\ldots, \tag{2}$$

where $k_{SPP}(\omega)=(2\pi/\lambda)\sqrt{\varepsilon_d\varepsilon_m/(\varepsilon_d+\varepsilon_m)}$ and $\varepsilon_m,\varepsilon_d$ are dielectric constants of the metal and dielectric (opal or air) at the interface.

The maximum at 725 nm [band 2 in Fig. 2(b)] corresponds exactly to the node of the SPP resonance branch that propagates along the opal-gold film interface. At oblique angles of incidence the long-wavelength edge of the passbands in *p*-polarized transmitted light follows the dispersion of $o\langle 11\rangle$ branches for SPP at the Au-opal interface [Fig. 3(c)]. The next set of SPP dispersion curves that belong to the air-gold film interface has its origin in the smaller transmission peak centered at 605 nm [band 4 in Fig. 2(b)]. At oblique angles of incidence the $a\langle 11\rangle$ SPP dispersions also associated with transmission passbands of the Au-opal hy-

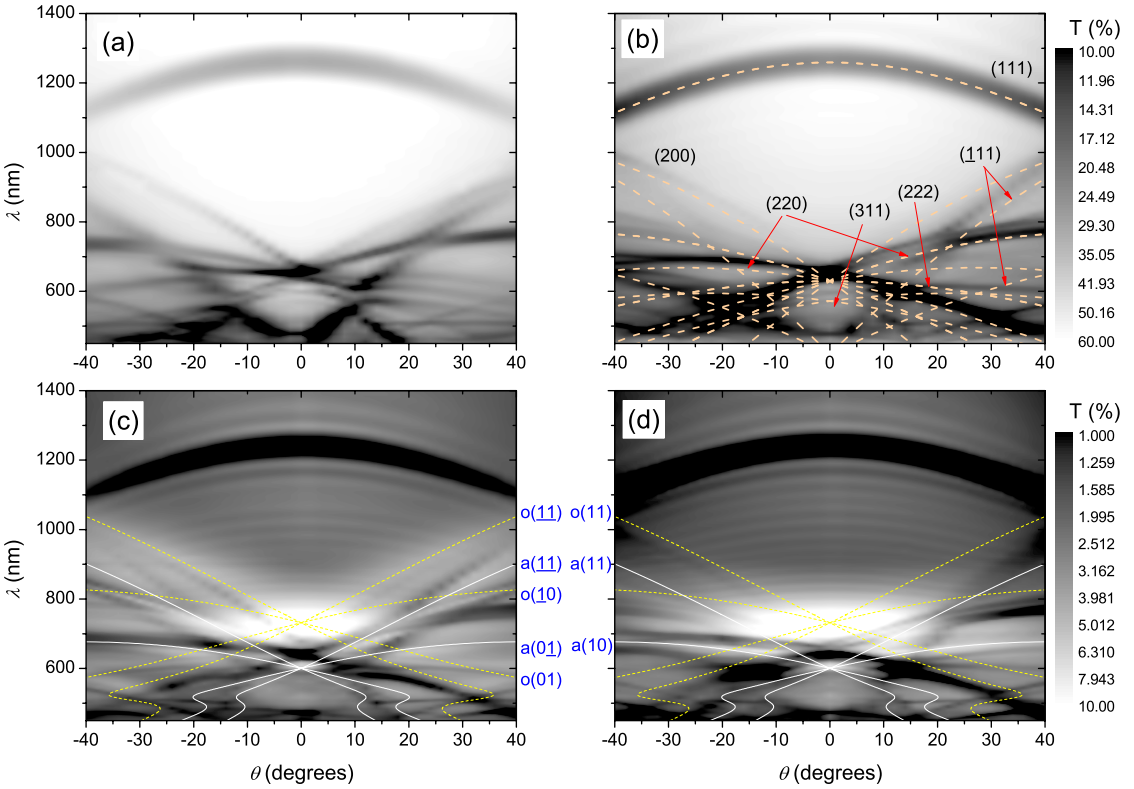

FIG. 3. (Color online) (a) and (b) Transmission patterns of the bare opal under *p*- and *s*-polarized light, respectively. Dashed lines denote the dispersion of diffraction resonances in fcc lattice. Numbers stand for Miller indices of respective lattice planes. (c) and (d) The transmission patterns of the Au-opal hybrid. Dashed and solid lines show the dispersion of SPP resonances at the opal-gold film (*o* modes) and air-gold film (*a* modes) interfaces.

brid. Thus, we can conclude that passbands in the *p*-polarized transmission of Au-coated opals correspond to the EOT in a metal film that is periodically corrugated and perforated with subwavelength holes [Fig. 1(b)].[14]

The angular dispersions of the passbands observed under *s*-polarized light differ from those under *p*-polarized light in a manner that is similar to the EOT polarization anisotropy reported in the lattice of subwavelength holes.[28] The dispersion of the latter bands is better approximated by $a\langle 10\rangle$ branches for SPP at the Au-air interface. Band 3 in Fig. 2(b), where the transmission experiences 20 times increase, is the EOT peak.

The observed EOT bands in the Au-opal hybrid crystal are similar to those reported for the EOT of Au-coated 2D PhC slabs consisting of a hexagonally packed monolayer of spheres.[21] Comprehensive numerical studies have demonstrated the direct connection between the EOT peak and the 2D PBG structure, linking not only the EOT peak position with the sphere diameter, but also assuming localization of the EM field in the eigenmodes of the 2D PhC as being the major cause for enhancing the EOT.

Overall, the "patchy" transmission pattern of the Au-opal hybrid PhC is determined by the dispersive transmission minima associated with diffraction resonances in the opal lattice and the coexisting dispersive transmission passbands associated with the SPP radiative decay in the corrugated metal coating on the opal crystal surface. Thus, we achieved the first aim of this study—the PhC with the surface capable of maintaining the surface modes that are disconnected from the PBGs.

IV. THREE-DIMENSIONAL EFFECTS IN THE HYBRID TRANSMISSION

Let us compare the transmission spectra acquired from the Au-opal hybrid structure to that of its parent opal film acquired at the same angles of incidence (Fig. 4). At $\theta=36°$ several transmission passbands are observed at wavelengths shorter than that of (111) resonance. First, the transmission sharply increases at the edge of the $o(\bar{1}\bar{1})$ SPP branch [Fig. 4(a)]. While the intensity of 887 nm transmission peak is only 4.5%, it remains some three times higher than the transmission at 1600 nm. The following minimum at 771 nm is due to (220) diffraction resonance. But the $(\bar{1}11)$ minimum is missed and replaced with transmission passband. Compared to the spectrum obtained in *p*-polarized light, the *s*-polarized transmission spectrum of the Au-opal hybrid structure replicates all diffraction minima of the bare opal and shows no transmission passbands until $\lambda > 745$ nm [Fig. 4(c)].

Along the mirrorlike angle of incidence $\theta=-36°$ the transmission spectra of both the bare opal and Au-opal hybrid change their appearances [Fig. 4(b)]. Projecting the transmission peaks in Fig. 4(b) onto Fig. 4(a) (dashed lines), one can immediately notice that passbands appear approximately at the same positions, whereas the diffraction resonances of the

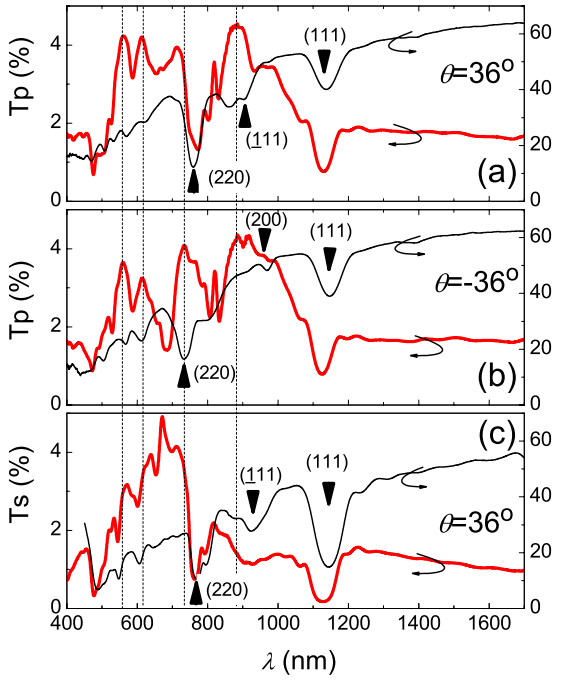

FIG. 4. (Color online) Transmission spectra of the bare opal (spheres, 560 nm) (thin line) and Au-opal hybrid (thick line) in p-polarized light at (a) $\theta=36°$ and (b) at $\theta=-36°$, and in s-polarized light at $\theta=36°$. Vertical dashed lines are to demonstrate the passband alignment. Numbers at arrows indicate the crystal planes for corresponding diffraction resonance.

bare opal change their locations. This observation points to the superposition of two systems of resonances in the spectra of the hybrid crystal. However, the linear superposition cannot explain, for example, why the (220) resonance at $\theta=36°$ corresponds to the minimum in spectrum of Au-opal, whereas the same resonance at $\theta=-36°$ is replaced with the transmission passband. The enhancement band 3 in Fig. 2(b) can be related to this mechanism.

Thus, we see that the transmission pattern of the Au-opal hybrid structure possesses a clear asymmetry with respect to reversing the sign of incidence angle [Figs. 1(b), 3(b), 3(c), 4(a), and 4(c)] in disagreement with the hexagonal symmetry of the (111) plane of the sphere lattice at the opal surface. In the first glance, the transmission pattern of the Au-opal hybrid crystal carries a trivial fingerprint of the transmission attenuation in the resonances of a 3D fcc opal lattice, the [111] axis of which does not have the twofold rotation symmetry axis. However, this asymmetry can also be linked to a distortion of the metal film profile and to the SPP excitation by the beams diffracted in 3D opal grating.

On one hand, the lack of mirror symmetry in the metal film profile can be a consequence of the 3D structure of the opal template used in the hybrid Au-opal structure. Figure 5 illustrates the reduction in the sixfold rotation symmetry axis in the metal lattice, when the actual shape of the metal coating on the surface of the opal film is taken into account. When metal penetrates the interstitials between touching spheres during sputtering process, it samples the depth of the cavity behind these windows. These cavities are either tetrahedral (between three spheres, characteristic size of $0.23D$) or octahedral (between six spheres, $0.41D$)[29] due to the shift of the second monolayer of spheres underneath the topmost one. Since this shift can be realized in two different ways, the hexagonal symmetry of a metal corrugation is reduced to a trigonal symmetry. Therefore, the corrugation of the metal film is distorted due to periodical interchange of the cavity size and, hence, it can be described by unit cells of the doubled size compared to the cells of a metal coating on top of a monolayer of hexagonally packed spheres. This doubling can be described by fractional modes in Eq. (2).

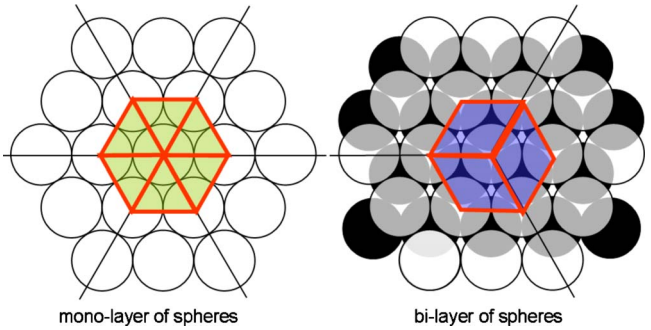

FIG. 5. (Color online) Schematics illustrating changing of the unit cell and symmetry of the 2D metal lattice if a 3D opal is used as a template for metal spattering instead of a monolayer of spheres.

On the other hand, the role of opal in hybrid structures is not limited to the formation of the metal film topology. The metal film in such hybrids becomes exposed to the EM field that is structured in Bloch modes in contrast to the plane-wave illumination of perforated metal films. In order to rectify the transmission changes introduced by the metal film deposition we constructed the ratio $T_{\text{hybrid}}/T_{\text{opal}}$ (Fig. 6). Surprisingly, in such a normalized transmission pattern the mirror asymmetry appears exaggerated instead of being washed

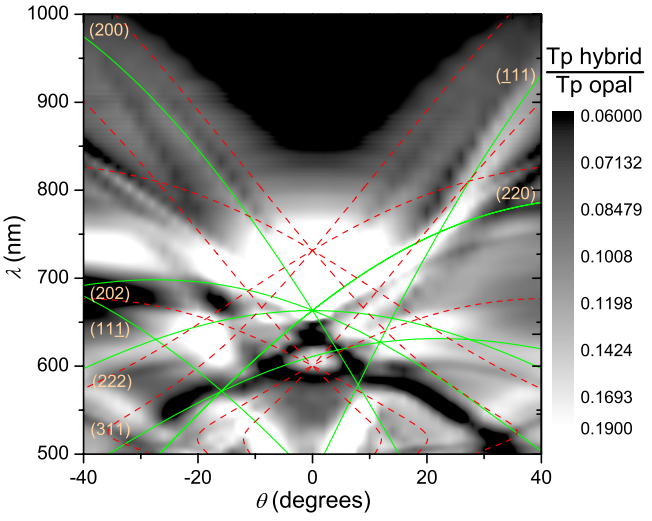

FIG. 6. (Color online) Ratio of p-polarized transmission spectra in the Au-opal hybrid and opal template. Dispersion of diffraction resonances in the fcc lattice of closed-packed spheres is shown by solid lines and labeled with Miller indices. SPP dispersions are shown by dashed lines. Brighter regions correspond to the relative enhancement of transmission.

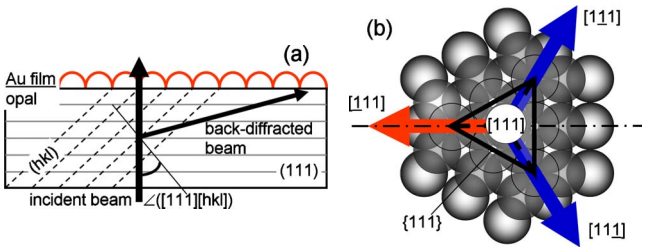

FIG. 7. (Color online) (a) Schematics illustrating the excitation of SPP waves by the (*hkl*) backdiffracted beam in the case of the incident beam directed along the opal film normal. Only one diffracted beam is shown for simplicity. If the angle between (111) and (*hkl*) planes is small, the backdiffracted beam cannot approach the Au film and couple to SPP. (b) Schematics illustrating zero-order diffraction resonances at ⟨111⟩ family of planes in the fcc lattice, for the incident beam propagating along the [111] axis that corresponds to the opal normal. Three (111) planes are shown along the [111] axis. Note that four ⟨111⟩ planes form a tetrahedron. If the incidence beam is rocked within the plane of incidence indicated by dashed-dotted line, only the diffracted beam [$\bar{1}$11] will stay in the plane of incidence.

out [compare Figs. 3(c) and 6], as it would be expected in the case of linear superposition of the opal and metal film spectra. In Fig. 6 one can distinguish two types of the relative transmission enhancement bands that follow the dispersions of SPP resonances in the 2D plasmonic crystal and the dispersion of diffraction resonances in the 3D opal lattice. Interestingly, only a selection of 3D resonances, like ($\bar{1}$11) and (200) resonances for *LK* scanning direction, gives rise to the transmission enhancement, whereas other 3D diffraction bands, e.g., (220) and (311) resonances, remain the transmission attenuation bands.

The bands of enhancement transmission are associated with grating-assisted coupling of photons to SPPs in a metal film. Coupling of incident light to SPP occurs due to imprinted corrugation of a metal film.[16] Excitation of SPP waves in a flat metal film by the light diffracted in attached dielectric grating is also a well-documented phenomenon.[30,31] In the first approximation, by disregarding the uneven distribution of light intensity to different diffraction orders, the diffraction in 3D grating does not excite any additional SPPs in the metal coating, because only tangential to the surface projection of the grating vector is useful in excitation of plasmon waves. Obviously, all projections of [*hkl*] vectors commensurate the [*hk*] vectors of surface lattice in one and the same 3D crystal [Fig. 7(a)].

Let the incident beam propagate along the [111] axis that is also the normal to the metal film. This beam will be diffracted by {*hkl*} planes of the lattice. Therefore, the Au film becomes exposed simultaneously to a number of beams, the incident one and its diffracted orders. The necessary condition for the observation of the enhanced transmission in our experimental conditions is the propagation of the incident and the outgoing beams with the same wave vector. The fulfillment of this condition is ensured by the same conditions for grating-assisted in-coupling and out-coupling of the light to or from SPP. This statement is consistent with the independence of transmission spectra on reversing the light propagation direction.

The schematics in Fig. 7(a) show the reason why the {*hkl*} crystal planes can be discriminated with respect to the angle, which they form with the (111) plane or the opal surface. For example, the interplane angle with ($\bar{1}$11) planes is $r_{\bar{1}11}$ = 70.53° and, hence, the zero-order backdiffracted beam hits the Au film if the incident beam is directed along the film normal. In this case both the incident and diffracted beams are able to excite the SPP. In contrast, because the angles between (220) and (311) planes with a (111) plane at the opal crystal surface are less than 45°, the backdiffracted beams cannot reach the metal coating for the same wavelength as those diffracted by ($\bar{1}$11) and (200) planes. In this case the transmission spectrum shows a minimum [Figs. 3(c) and 6].

As illustrated in Fig. 7(b) using the example of diffraction at {111} planes, if the incident beam hits the opal surface along the film normal, all corresponding diffracted beams will be able to excite the SPP and contribute to transmission enhancement with the same efficiency. However, if the incident beam will be rocked in the plane of incidence, indicated by the dashed-dotted line, the beam [$\bar{1}$11] will approach the surface at different angles compared to beams [1$\bar{1}$1] and [11$\bar{1}$]. Since the corresponding diffraction pattern lacks the mirror symmetry, if the incident beam will change the direction of its inclination with respect to the [111] film normal,

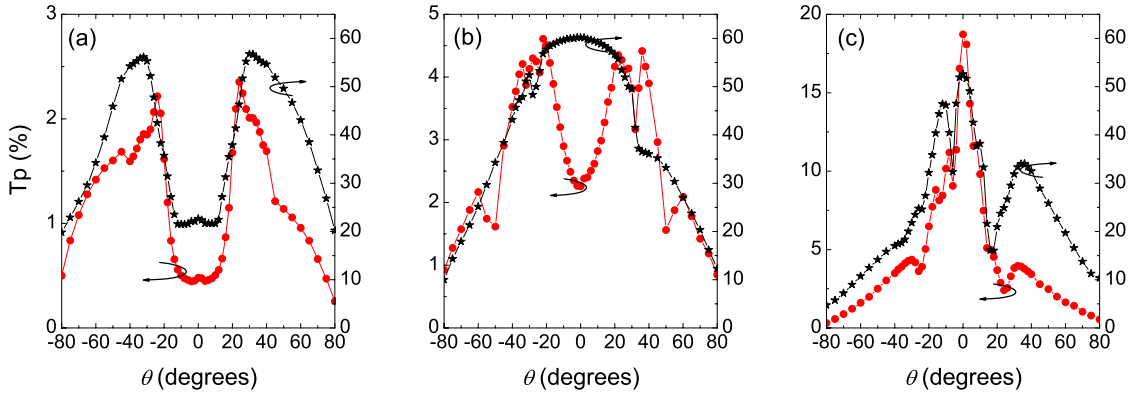

FIG. 8. (Color online) Angular diagrams of transmission of the opal film (D=560 nm) (stars) and Au-opal hybrid (circles) obtained at (a) 1240, (b) 900, and (c) 725 nm.

the SPP pattern will acquire the corresponding asymmetry with respect to changing the sign of the incidence angle. Our experiment with the Au-opal hybrid structure shows that the transmission pattern of the Au-opal hybrids acquires the symmetry related to that of 3D opal lattice both in terms of transmission attenuation and enhancement.

V. TRANSMISSION INDICATRIX

The obvious consequence of overlaying the angular dependence of the EOT intensity in a metal coating and diffraction resonances in 3D PhC is the dramatic change in the angular transmission diagrams of the Au-opal hybrid as compared to the same diagrams for the parent opal. Since the transmission diagram in an opal crystal is controlled by diffraction resonances, this leads to a variation of the diagram as a function of wavelength. However, in the case of moderate refractive index contrast, the angular bandwidth of the diffraction resonance is not large enough to suppress transmission over a broad angle range. This case is illustrated in Fig. 8(a), where the most broadband (111) resonance provides a suppression of the transmission only within a 25°-wide angle interval. In the spectral range away from the EOT resonance, the diagram of the hybrid sample shows the same behavior, except for the much lower transmission magnitude and the edge sharpening occurring due to the presence of a long-wavelength transmission passband [band 1 in Fig. 2(b)], which will be discussed in the next section.

The dissimilarity of the diagrams for the Au-opal hybrid and the parent opal in the spectral range around 800–900 nm is the consequence of SPP transmission passbands [Fig. 8(b)]. In the range of the main EOT band, the angular diagram of transmission in the hybrid sample shows a synergy between the EOT intensity reduction along the angle increase and the transmission suppression by diffraction resonances. The diffraction effect is clearly indicative of the transmission diagram asymmetry inherited from a 3D fcc crystal, which does not possess the twofold rotation axis [Fig. 8(c)]. The observed transmission diagram, which reveals a peak spanning at approximately 20°, would be expected to further sharpen (i.e., its angular width would reduce) in the case of stronger attenuation by diffraction resonances, e.g., in thicker opal films. It is important to mention that in the EOT range the difference between transmissions of bare and Au-coated opal samples is strongly reduced compared to other spectral intervals. This "bladelike" profile of transmission indicatrix is a kind of beaming the transmitted light, which is achieved without the use of an aperture and is the result of applying the nearly "loss-free" approach to beam profile engineering.

VI. TRANSMISSION VERSUS METAL COATING THICKNESS

The development of transmission spectra of hybrid structures with the increasing thickness of Au film sets the limits for transmission spectrum engineering by varying the metal coating. From Fig. 9(a) one can conclude that (i) thin coating acts as a screen that overlays the transmission of the metal film on top of the spectrum of the opal template; (ii) the moderately thick coating substantially reduces transmission and favors the sharp SPP resonance while maintaining the well-resolved transmission minima; and (iii) thick coating suppresses the transmission dramatically, retains weak SPP-related peak, and shows additional resonance features.

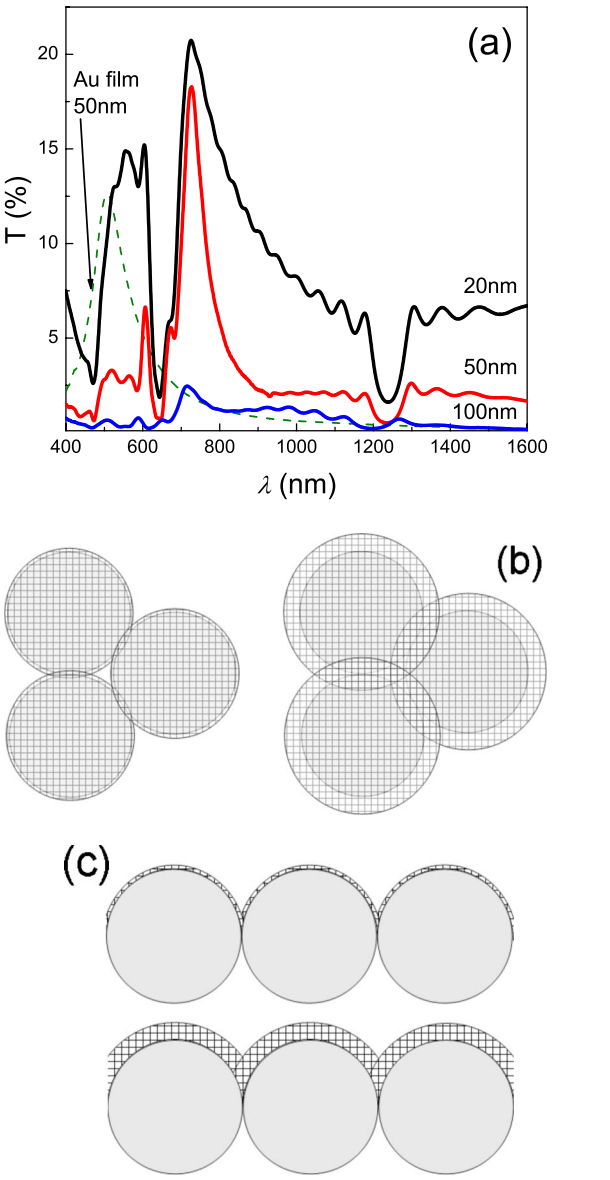

FIG. 9. (Color online) (a) Transmission spectra of Au-opal (560 nm, spheres) with Au coating of different thicknesses that are indicated at curves. Dashed line shows the transmission spectrum of the 50-nm-thick Au film. (b) Top and (c) cross-section side schematic views of a metal layer coating (square patterned area) on the opal surface for different coating thicknesses.

The transmission maps of Au-opal hybrid crystals with different coating thicknesses (Fig. 10) that are obtained in a broad angle range support these observations. These maps show a common feature—the transmission peak at the nodes of the 2D SPP dispersion branches. However, the fraction of the map area that shows the transmission enhancement varies dramatically with increasing coating thickness. One can see that the 20-nm-thick coating does not lead to the formation of pronounced passband with characteristic 2D SPP disper-

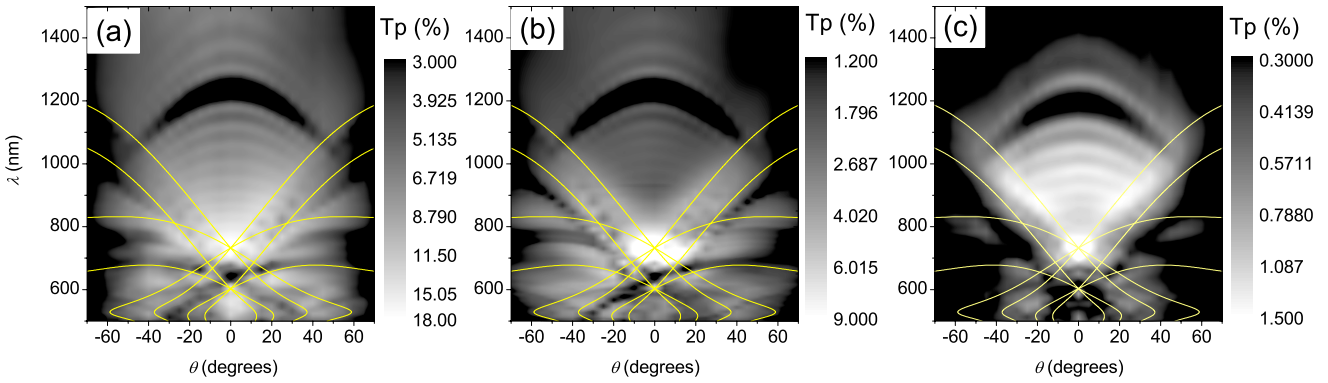

FIG. 10. (Color online) Transmission patterns of hybrid opals assembled from 560 nm spheres under *p*-polarized light with Au coating thicknesses of (a) 20, (b) 50, and (c) 100 nm. Calculated dispersions of SPP eigenmodes are overplayed.

sion that is present in the transmission map of the hybrid structure with 50-nm-thick coating. Moreover, the map in Fig. 10(b) shows the asymmetry with respect to reversing the incidence angles, whereas the map in Fig. 10(a) is almost symmetrical. In contrast, the hybrid with 100-nm-thick coating not only supports the $o\langle 11\rangle$ and $a\langle 11\rangle$ SPP bands, but also shows a substantial transmission enhancement in the area between them, where the enhancement can be assigned neither to 2D nor to 3D SPP grating coupling. It is important to emphasize that $(\bar{1}11)$ and (200) transmission minima cannot be traced in the case of thick Au coating in contrast to that in the case of thin metal coating, while (220) minima are clearly resolved in both maps [compare Figs. 10(a) and 10(c)]. This observation recalls the mechanism of SPP excitation by 3D grating illustrated in Fig. 7.

In order to interpret these variations we should take into account that the increase in the metal film thickness leads to changing the topology of the metal film from nearly isolated metal caps on top of opal spheres to continuous films with much shallower corrugation [Figs. 9(b) and 9(c)]. Apparently, excitation of propagating SPP waves in the case of thin coating is extremely inefficient due to the very deep profile and poor connectivity of metal caps. Instead, individual resonances can be excited in these caps.[32]

In the 100-nm-thick film coating, the through holes are closed because caps on adjacent spheres overlap each other [Figs. 9(b) and 9(c)]. In this case the coupling strength between SPPs across the metal film is reduced, whereas the depth of the corrugation remains high and SPP can be efficiently scattered. It is instructive to mention here that the optimum coupling of SPPs can be achieved if the corrugation depth is ~10% relative to the period.[33] Combination of these factors reduces dramatically the hybrid structure transparency and also suppresses the EOT, thus bringing the structure closer to the mirror case.

At long wavelengths the transmission of planar 50-nm-thick Au film is lower than that of Au-opal counterpart in spite of ~60% transparency of the bare opal [Fig. 9(a)]. There are two reasons for this difference. On one hand, the thickness of the metal coating is unevenly distributed on the surface of the opal substrate that reduces the reflectivity of the Au coating compared to the planar film. On the other hand, the opal film acts as the antireflection coating,[34] thus increasing the hybrid transparency. This mechanism explains the increase in the normalized transmission of the opal hybrid with 50 nm Au coating toward long wavelengths [Fig. 2(b)] and it also applies to other samples in Fig. 10.

The opal, however, is not a piece of a homogeneous dielectric and also acts in the range of (111) diffraction resonance as the Bragg mirror, which is attached to the metal mirror. In this case the surface wave can be maintained between two mirrors—the opal film and the metal coating—which mode is seen as a peak in transmission spectrum.[35] Band 1 in Fig. 2(b) can be assigned to this mechanism, which is not related to the excitation of SPP but, nevertheless, appears as the result of the resonance cavity formation. With increasing coating thickness this mechanism becomes more efficient, because the metal film reflectivity increases. We assume that this mechanism is responsible for the increased transparency of the hybrid structure with 100-nm-thick Au coating in the spectral range from 900 to 1300 nm in the angle range between SPP bands [Figs. 9(a) and 10(c)]. In this broad range the light in the opal is coupled to PhC eigenmodes, the properties of which differ from the modes of the free space. The uncoupled light in this case can also be confined at the opal-metal interface. The idea of stronger light confinement in the opal film in this range is supported by the increase in the magnitude of the Fabry-Pérot fringes over the transmission enhancement band centered at 1000 nm.

VII. CONCLUSIONS

In summary, we described a photonic platform, the 3D PhC-based hybrids, in which the metal at the crystal surface plays a crucial role in the formation of optical properties of PBG material in a broad spectral range. We therefore emphasize that the observed sharp resonance structure of the transmission pattern in such hybrid architectures is, mostly, a result of synergetic action of the 2D SPP-BG structure[36] and the 3D PBG material.

The optical transmission of a hybrid Au-coated opal crystal accumulates minima related to diffraction resonances in the 3D lattice; the EOT passbands are related to the radiative decay of eigenmodes in a 2D SPP band-gap crystal and the passband due to the cavity mode in the range of the first opal

band gap. Thus, the extended functionality of the Au-opal hybrid crystals is based on three resonance mechanisms compared to the only one behind the operation of the dielectric opal crystals.

The rich variety of the optical phenomena involved in the formation of optical properties of these hybrid metal-dielectric colloidal crystals can be exploited in order to enable further engineering the transmission and reflectance functions of photonic crystals. Taking into account low light dissipation in a metal film, such architectures can be attractive for the design of PhC-based light sources and light trapping in photovoltaic devices.

ACKNOWLEDGMENTS

A.V.K., U.P., and S.G.R. are grateful to DFG Cluster of Excellence "Engineering of Advanced Materials" (Germany) for financial support, B.D. was supported by the SFI Grant No. RFP PHY076 (Ireland), and M.E.P. acknowledges SFI Grant No. PI 07/IN.1/1787 (Ireland). Both groups are linked through the COST Action Grant No. MP0702. The authors acknowledge J. McGrath for taking SEM pictures.

*Corresponding author; sergei.romanov@mpl.mpg.de

[1] K. Ishizaki and S. Noda, Nature (London) **460**, 367 (2009).
[2] A. Tikhonov, J. Bohn, and S. A. Asher, Phys. Rev. B **80**, 235125 (2009).
[3] R. Moussa, B. Wang, G. Tuttle, Th. Koschny, and C. M. Soukoulis, Phys. Rev. B **76**, 235417 (2007).
[4] R. D. Meade, K. D. Brommer, A. M. Rappe, and J. D. Joannopoulos, Phys. Rev. B **44**, 10961 (1991).
[5] W. M. Robertson, G. Arjavalingam, R. D. Meade, K. D. Brommer, A. M. Rappe, and J. D. Joannopoulos, Opt. Lett. **18**, 528 (1993).
[6] S. Xiao, M. Qiu, Z. Ruan, and S. He, Appl. Phys. Lett. **85**, 4269 (2004).
[7] N. Stefanou, V. Yannopapas, and A. Modinos, Comput. Phys. Commun. **113**, 49 (1998).
[8] S. G. Romanov, H. M. Yates, M. E. Pemble, and R. M. De La Rue, J. Phys.: Condens. Matter **12**, 8221 (2000).
[9] E. Istrate and E. H. Sargent, Rev. Mod. Phys. **78**, 455 (2006).
[10] A. V. Kavokin, I. A. Shelykh, and G. Malpuech, Phys. Rev. B **72**, 233102 (2005).
[11] B. Ding, M. Bardosova, I. Povey, M. E. Pemble, and S. G. Romanov, Adv. Funct. Mater. **20**, 853 (2010).
[12] J. C. Hulteen and R. P. Van Duynea, J. Vac. Sci. Technol. A **13**, 1553 (1995).
[13] Z.-B. Wang, Y.-H. Ye, Y.-A. Zhang, and J.-Y. Zhang, Appl. Phys. A: Mater. Sci. Process. **97**, 225 (2009).
[14] T. W. Ebbesen, H. J. Lezec, H. F. Ghaemi, T. Thio, and P. A. Wolff, Nature (London) **391**, 667 (1998).
[15] W. L. Barnes, A. Dereux, and T. W. Ebbesen, Nature (London) **424**, 824 (2003).
[16] S. A. Maier, *Plasmonics: Fundamentals and Applications* (Springer, New York, 2007).
[17] Y.-S. Shon, H. Y. Choi, M. S. Guerrero, and C. Kwon, Plasmonics **4**, 95 (2009).
[18] P. Zhan, Z. Wang, H. Dong, J. Sun, J. Wu, H.-T. Wang, S. Zhu, N. Ming, and J. Zi, Adv. Mater. **18**, 1612 (2006).
[19] L. Landström, D. Brodoceanu, K. Piglmayer, and D. Bäuerle, Appl. Phys. A: Mater. Sci. Process. **84**, 373 (2006).
[20] C. Farcau and S. Astilean, J. Opt. A, Pure Appl. Opt. **9**, S345 (2007).
[21] L. Landström, D. Brodoceanu, D. Bäuerle, F. J. Garcia-Vidal, S. G. Rodrigo, and L. Martin-Moreno, Opt. Express **17**, 761 (2009).
[22] M. Müller, R. Zentel, T. Maka, S. G. Romanov, and C. M. Sotomayor Torres, Chem. Mater. **12**, 2508 (2000).
[23] W. Khunsin, G. Kocher, S. G. Romanov, and C. M. Sotomayor Torres, Adv. Funct. Mater. **18**, 2471 (2008).
[24] P. B. Johnson and R. W. Christy, Phys. Rev. B **6**, 4370 (1972).
[25] B. R. Cooper, H. Ehrenreich, and H. R. Philipp, Phys. Rev. **138**, A494 (1965).
[26] W. Khunsin, A. Amann, and S. G. Romanov (unpublished).
[27] F. García-Santamaría, J. F. Galisteo-López, P. V. Braun, and C. López, Phys. Rev. B **71**, 195112 (2005).
[28] H. F. Ghaemi, Tineke Thio, D. E. Grupp, T. W. Ebbesen, and H. J. Lezec, Phys. Rev. B **58**, 6779 (1998).
[29] V. G. Balakirev, V. N. Bogomolov, V. V. Zhuravlev, Y. A. Kumzerov, V. P. Petranovskii, S. G. Romanov, and L. A. Samoilovich, Crystallogr. Rep. **38**, 348 (1993).
[30] K. G. Müller, M. Veith, S. Mittler-Neher, and W. Knoll, J. Appl. Phys. **82**, 4172 (1997).
[31] X. Li, D. Han, F. Wu, C. Xu, X. Liu, and J. Zi, J. Phys.: Condens. Matter **20**, 485001 (2008).
[32] A. I. Maaroof, M. B. Cortie, N. Harris, and L. Wieczorek, Small **4**, 2292 (2008).
[33] I. Ursu, I. N. Mihailescu, A. M. Prokhorov, V. I. Konov, and V. N. Tokarev, Physica B & C **132**, 395 (1985).
[34] D. Han, X. Li, F. Wu, X. Liu, and J. Zi, Appl. Phys. Lett. **88**, 161110 (2006).
[35] A. S. Ramírez-Duverger, J. Gaspar-Armenta, and R. García-Llamas, J. Opt. Soc. Am. B **25**, 1016 (2008).
[36] S. C. Kitson, W. L. Barnes, and J. R. Sambles, Phys. Rev. Lett. **77**, 2670 (1996).